IET Nanobiotechnology

*Research Article*

IET Journals
The Institution of Engineering and Technology

# Dual application of *Shewanella oneidensis* MR-1 in green biosynthesis of Pd nanoparticles supported on $TiO_2$ nanotubes and assisted photocatalytic degradation of methylene blue

ISSN 1751-8741
Received on 5th June 2017
Revised 29th November 2017
Accepted on 13th December 2017
E-First on 28th February 2018
doi: 10.1049/iet-nbt.2017.0130
www.ietdl.org

*Xiaojie Song[1,2], Xianyang Shi[1] ✉, Mi Yang[1]*

[1]*School of Resource and Environmental Engineering, Anhui University, Hefei 230601, People's Republic of China*
[2]*School of Materials and Chemical Engineering, Anhui Jianzhu University, Hefei 230601, People's Republic of China*
✉ *E-mail: shixi381@163.com*

**Abstract:** Biosynthesised nanocomposites have attracted growing interests attributed to their 'green' synthesis nature in recent years. *Shewanella oneidensis* MR-1, a dissimilatory metal-reducing bacterium, was used to reduce palladium (II) nitrate to palladium (0) nanoparticles (Pd NPs) under anaerobic conditions, resulting in the in situ formation of Pd NPs immobilised on $TiO_2$ nanotubes (TNTs) (Pd/TNTs nanocomposites). The Pd/TNTs nanocomposites were characterised by transmission electron microscopy, X-ray diffraction, X-ray photoelectron spectroscopy, energy dispersive X-ray, and electron spin resonance, respectively. The results indicated that Pd NPs are successfully grown on the TNTs without aggregation. Photocatalytic degradation of methylene blue (MB) by Pd/TNTs nanocomposites under simulated sunlight was also investigated. Pd/TNTs nanocomposites had photocatalytic efficiency superior to that of single $TiO_2$ nanomaterials. The photocatalytic activity of Pd/TNTs nanocomposites can be enhanced by *S. oneidensis* MR-1. The results showed that after only 10 min, the degradation ratio of MB reached 98.7% by Pd/TNTs nanocomposites when simultaneously assisted with *S. oneidensis* MR-1.

## 1 Introduction

*Shewanella oneidensis* widely distributed in environments is intensively studied for the bioremediation of environmental contaminants [1]. It has been used for the reduction of numerous metals [2–4] and metal sulphide due to its considerable reductive capacity [5]. One-dimensional TNTs have been broadly utilised as photocatalytsts because of their advantages, such as exhibiting the same order of magnitude as their absorption wavelength in the ultraviolet (UV) region, large surface-to-volume ratio and direct pathways for charge transport and rich activity sites [6, 7]. All of these advantages provide TNTs with better photocatalytic efficiency than traditional $TiO_2$ nanoparticles ($TiO_2$ NPs). However, there are still several common drawbacks, including its wide band gap and the high recombination rate of photoexcited electron–hole pairs, which restrict the wide application of TNTs in photocatalysis [8, 9].

To overcome these drawbacks, a variety of materials are introduced on $TiO_2$ to yield heterogeneous photocatalysts [10, 11] that can offer several potential benefits: first, the utilisation of light is enhanced in a larger range from UV light to visible light; second, heterostructures at the interface of heterogeneous photocatalysts create a built-in electrical potential, which can reduce the recombination of electron–hole pairs [12]. The doping of noble metal nanoparticles such as Au, Ag, Pt and Pd is a valuable option [13–15]. Through irradiating noble metal nanoparticles with UV light/visible light, intense electric fields are generated which promote the generation of photoexcited electrons [16]. Meanwhile, the Schottky barrier at the interface of noble metal/$TiO_2$ effectively enhances the electron–hole pair separation and transfer [12]. Among the noble metals, Pd is chosen because of its relatively low cost and high work function, which favours the electrons transfer [17].

Conventional approaches [18, 19] to the synthesis of these nanoparticles are generally accompanied by the use of toxic or dangerous chemicals and high consumption of energy under extreme conditions. The bio-inspired approach can synthesise the nanomaterials under mild conditions and fewer chemicals are involved in the production process. So far, little information is available about to heterogeneous photocatalysts synthesised by *S. oneidensis* MR-1 and their application in the photocatalytic degradation of methylene blue (MB).

In this present study, we wanted to combine the green synthesis of nanomaterials by *S. oneidensis* MR-1 with their use in environmental bioremediation. Pd NPs were fabricated on TNTs in situ by a reducing agent, *S. oneidensis* MR-1. The morphology and characterisation of the structure of the Pd/TNTs nanocomposites were explored. The photocatalytic activity of the as-prepared Pd/TNTs nanocomposites with the synergistic effects of *S. oneidensis* MR-1 was evaluated according to the degradation capability for MB. The results of our work provide a simple, environmentally benign and cost-effective route for the fabrication of the noble metal/TNTs nanocomposites with well-defined nanocrystalline structure.

## 2 Experimental

### 2.1 Materials

*Palladium nitrate* (Pd $(NO_3)_2{\cdot}xH_2O$) and anatase $TiO_2$ powder (99.8%, ~25–30 nm in diameter) were obtained from Aladdin Chemistry Co., Ltd. (Shanghai, China).

Polyvinylpyrrolidone (PVP) and sodium dodecyl benzene sulfonate (SDS) were all analytically pure. These reagents were used directly without any further purification. Pd $(NO_3)$ solution was prepared by dissolving it in a modified basal mineral medium (MBMM), which was composed of 20 mM HEPES (*N*-(2-hydroxyethyl) piperazine-*N*′-2-ethanesulfonic acid) and 10 mL of a stock solution of the trace elements in each litre, with the pH being adjusted to 7 using sodium hydroxide. The detailed compositions of trace elements can be found elsewhere [11].

A single bacterial colony of *S. oneidensis* MR-1 from an overnight culture in Luria–Bertani (LB) medium was inoculated into serum bottles containing 100 mL of LB medium at 30°C on a

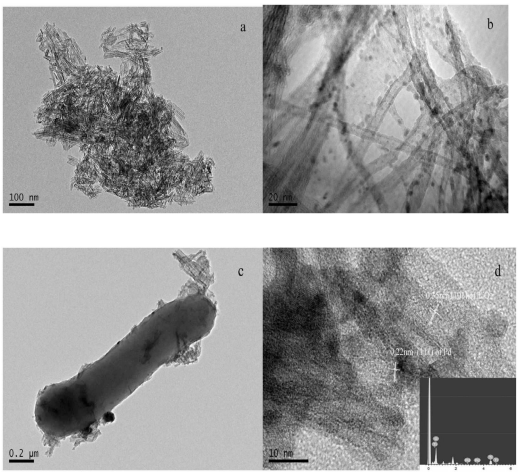


**Fig. 1** *TEM images*
***(a)*** TNTs, ***(b)*** Pd/TNTs nanocomposites (1 wt% of Pd), ***(c)*** Pd/TNTs nanocomposites and *S. oneidensis* MR-1, ***(d)*** HRTEM image of Pd/TNTs nanocomposites (The inserted figure is EDS image of Pd/TNTs nanocomposites.)

shaker (150 rpm) for 24 h. The bacteria were collected in their later stationary phase by centrifugation (6000 rpm, 20 min) and washed with MBMM three times under sterile conditions.

### 2.2 Preparation of TNTs

TNTs were synthesised via a simple hydrothermal process [20] without the use of an autoclave. Typically, 2 g of commercial anatase $TiO_2$ powder was added to 100 mL of 10 mol $L^{-1}$ NaOH, and the mixture was refluxed for 48 h at 120°C. The resulting product was diluted with distilled water before filtration. The collected titania nanotubes were rinsed twice by stirring overnight with 0.1 mol $L^{-1}$ HCl at 70°C and was thoroughly rinsed with distilled water. The TNTs were then prepared by an annealing at 400°C for 1 h.

### 2.3 Synthesis of Pd/TNTs nanocomposites

SDS was dissolved in 25 mL of MBMM resulting in a concentration of 1 wt%, followed by the addition of a certain amount of TNTs and 300 mg of PVP with vigorous stirring for 4 h at room temperature. Finally, *palladium nitrate* was added to the dispersed TNTs solution.

The sterilised MBMM was sparged with $N_2$ for 10 min to remove dissolved $O_2$ from the serum vials, and 2 mL of the above *palladium nitrate*/TNTs turbid liquid was subsequently injected into the MBMM through a sterile syringe. After that, the collected *S. oneidensis* MR-1 were inoculated into the serum vials through a sterile syringe resulting in an initial cell density of $5 \times 10^6$ CFU $mL^{-1}$. All serum vials were cultured on a 150 rpm shaker at 30°C. At the end of the process (120 h), the reaction mixture was first centrifuged (5000 rpm, 20 min) to remove the bacteria, and the Pd/TNTs nanocomposites were subsequently harvested by high-speed centrifugation (10,000 rpm, 20 min) using an ultracentrifuge. The collected nanocomposites were washed twice with deionised water and ethanol and finally dried at 60°C for 24 h. Three kinds of Pd/TNTs nanocomposites with different mass *percentages* of Pd (1, 4 and 8 wt%) were prepared to compare their photocatalytic capacity.

### 2.4 Characterisation

Morphology and particle size were observed using energy dispersive X-ray (EDS) analysis and transmission electron microscopy (TEM). Powder X-ray diffraction (XRD) spectra were obtained using a Bruker D8-Advance X-ray diffractometer with a Cu Kα source ($\lambda = 1.54178$ Å). X-ray photoelectron spectroscopy (XPS) was performed using a Rigaku SmartLab electron spectrometer. UV–vis absorption spectra were measured with a Lambda 900 UV–vis spectrophotometer (Perkin-Elmer) operated at a resolution of 1 nm. The electron spin resonance (ESR) spectra were obtained using a JEOL (JES-FA200) instrument with a sensitivity of $7 \times 10^9$ spins·$(0.1\ mT)^{-1}$.

### 2.5 Photocatalytic activity

The photocatalytic activity of the Pd/TNTs nanocomposites was evaluated by the degradation of MB solution at ambient temperature and pressure. A 300 W iodine-tungsten lamp with a wavelength range from 350 to 1000 nm was chosen to simulate a sunlight source. In a typical experiment, 25 mg of photocatalysts was dispersed in 50 mL of 40 mg/L MB solution, and the suspension was subsequently stirred for 1 h in the dark to reach the adsorption equilibrium. Next, the suspension was irradiated for 1 h under the iodine-tungsten lamp. At a defined time interval, the MB concentration was analysed at 664 nm using UV–vis spectrophotometer. The photocatalytic activities of $TiO_2$ NPs, TNTs, *S. oneidensis* MR-1, Pd/TNTs nanocomposites and Pd/TNTs nanocomposites with *S. oneidensis* MR-1 were determined under the same conditions. As a comparison, a blank experiment was also conducted without any photocatalyst.

## 3 Results and discussion

### 3.1 Characterisation of Pd/TNTs nanocomposites

The morphology and structure of TNTs, Pd/TNTs nanocomposites and *S. oneidensis* MR-1 are shown in Fig. 1. As shown in Fig. 1a, the TNTs are a typical nanotube structure with a uniform outer diameter of ∼10 nm and a length of approximate 100–200 nm. The formation mechanism of TNTs is proposed as follows [21]. Through the treatment of anatase $TiO_2$ in 10 M NaOH at 120°C, the layer-structured intermediate product $Na_2Ti_3O_7$ is formed, and then $Na^+$ ions are gradually replaced by water molecules in the hydrothermal process. Due to this replacement, the layered titanate particles exfoliate, and single nanosheets curl up to produce TNTs in their final form. In Fig. 1b, Pd NPs with a diameter of ∼6–8 nm are uniformly loaded on the surface of TNTs. Fig. 1c exhibits the formation of Pd/TNTs nanocomposites with the help of *S. oneidensis* MR-1. Many TNTs are adsorbed on the cell wall of *S. oneidensis* MR-1. The surface of some TNTs is blank, but a small amount of Pd NPs emerges on the surface of other nanotubes. In the synthesis process for the nanoparticles, *S. oneidensis* MR-1 plays an important role as electron donor. Electrons are generated in *S. oneidensis* MR-1 and are transmitted from the cytoplasmic membrane to the extracellular TNTs via an important anaerobic respiratory pathway constructed with the MtrA-MtrB-MtrC gene cluster of *S. oneidensis* MR-1 [5]. Since SDS is an anionic surfactant, $Pd^{2+}$ ions can be attracted to the wall of the TNTs easily and then accept the electrons and finally form Pd NPs. The HRTEM image (Fig. 1d) of the Pd/TNTs nanocomposites displays the region of the interface between the Pd NPs and TNTs. The lattice fringe spacing between two adjacent crystal planes of the nanotubes was determined to be 0.35 nm, corresponding to the (101) lattice plane of anatase. The lattice fringe spacing of 0.22 nm is attributed to the (111) lattice plane of Pd (0) [22–24]. The EDS spectrum (inserted figure of Fig. 1d) confirms that three elements, O, Ti and Pd, which come from TNTs and Pd NPs, also exist in the Pd/TNTs nanocomposites. These results imply that high-purity Pd/TNTs nanocomposites with heterostructures are successfully formed.

Fig. 2 shows the XRD patterns of TNTs and Pd/TNTs nanocomposites (1 wt% of Pd). The diffraction peaks at $2\theta = 25.6°$, 37.7° and 47.8° appeared in both patterns of TNTs and Pd/TNTs nanocomposites and can be associated with the (101), (004) and (200) planes, respectively, of anatase phase $TiO_2$ (JCPDS No.12-1272). No characteristic diffraction peak of Pd is detected in the XRD patterns of Pd/TNTs nanocomposites due to the small particle size and low loading amounts of Pd NPs [25]. On the other hand, the characteristic peak belonging to Pd (JCPDS No.02-1439) at 48.1° overlaps the (200) diffraction of anatase $TiO_2$.

XPS is used to obtain information (existence and valence state) of Pd and Ti on the surfaces of Pd/TNTs nanocomposites (1 wt% of

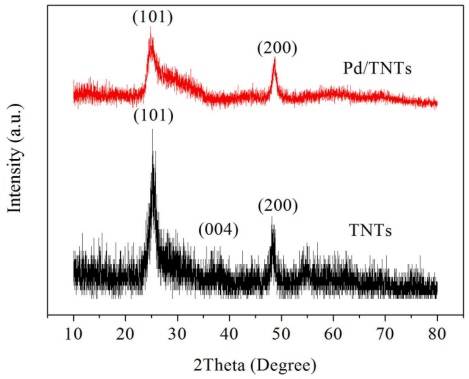


**Fig. 2** *XRD patterns of TNTs and Pd/TNTs nanocomposites (1 wt% of Pd)*

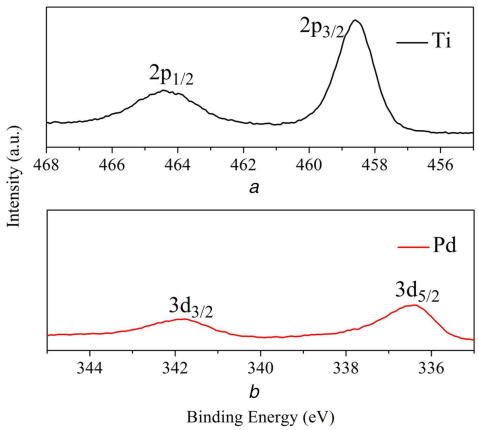


**Fig. 3** *High-resolution XPS spectra*
***(a)*** Ti 2p, ***(b)*** Pd 3d of Pd/TNTs nanocomposites (1 wt% of Pd)

Pd). The high-resolution XPS spectra of Ti 2p and Pd 3d are shown in Figs. 3a and b, respectively. In Fig. 3a, two binding energies at 464.5 and 458.7 eV are ascribed to the Ti $2p_{1/2}$ and Ti $2p_{3/2}$ orbitals, respectively, and the peak at 458.7 eV is ascribed to the $Ti^{4+}$ in $TiO_2$[26]. The binding energies at 336.4 and 341.8 eV in Fig. 3b are ascribed to $3d_{5/2}$ and $3d_{3/2}$ of Pd (0), respectively, which confirm the successful doping of Pd (0) on the TNTs. The distance between the two peaks is 5.4 eV, which further confirms the metallic Pd (0) is the only phase of palladium in present [17, 27].

The ESR spectroscopy method using 5,5-dimethyl-1-pyrroline N oxide (DMPO) as a spin-trapping reagent has been widely accepted as an efficient method to measure hydroxyl radical (•OH) formation. The ESR spectra for TNTs, Pd NPs and Pd/TNTs nanocomposites (1 wt% of Pd) under visible light irradiation are shown in Fig. 4. No obvious spectrum signature for TNTs is observed, indicating that single TNTs cannot adsorb visible-light to drive photochemical redox reactions. In contrast, there is a strong spectrum signature for Pd NPs and Pd/TNTs nanocomposites with an intensity ratio of 1:2:2:1, suggesting that hydroxyl radicals (•OH) are largely formed by the Pd NPs and they further reacts with MB, resulting in photocatalytic degradation. The spectral signature for Pd/TNTs nanocomposites is clearly stronger than that for single Pd NPs, indicating that TNTs play a highly important role in the enhancement of photocatalysis for Pd/TNTs nanocomposites. By comparing the ESR results among single TNTs, Pd NPs and Pd/TNTs nanocomposites, Pd/TNTs nanocomposites clearly have a wider utilisation range and stronger utilisation efficiency for sunlight in photocatalysis.

According to the local electric-field enhancement mechanism, intense electric fields form on the surfaces of nanomaterials through the absorption of photons by metal nanoparticles [16, 28]. The great enhancement of the intensity of the electric fields of local plasmonic 'hot spots' affirmed by the finite-difference time-domain method promote the generation of photoinduced charge locally in $TiO_2$. The doping of Pd NPs on TNTs not only realises

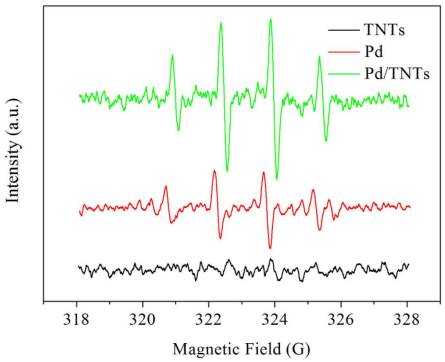


**Fig. 4** *Hydroxyl radical ESR spectra of Pd/TNTs nanocomposites (1 wt% of Pd), pure Pd NPs, and pure TNTs formed in aqueous dispersions in a Pyrex vessel containing ~20 mg sample after 5 min irradiation by visible light (filter: λ > 450). In the system, the concentration of DMPO is 0.4 mol $L^{-1}$*

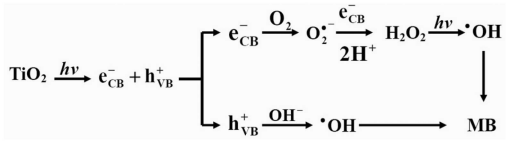


**Fig. 5** *Scheme 1: Formation of hydroxyl radicals and degradation of MB*

the local electric field enhancement but also reduces the band gap of TNTs to utilise visible light. Through absorption of visible light with an appropriate frequency, photo-excited electron–hole pairs ($e^-$–$h^+$) are generated in TNTs. Since the work function of Pd NPs (~5.2 eV) is higher than the electron affinity of anatase $TiO_2$ (~4.2 eV) [12], photo-excited electrons transfer from the conduction bands of TNTs to Pd NPs and a Schottky barrier at the interface of TNTs and Pd NPs reduces the recombination of electron–holes. The holes transfer to the surface of TNTs and react with hydroxyl ions in solution to form hydroxyl radicals (•OH). In contrast, the electrons on Pd NPs can also transform into hydroxyl radicals (•OH) through several reactions with dissolved $O_2$ [14]. As a strong oxidant, these hydroxyl radicals (•OH) react with MB to realise photocatalytic degradation. The formation of hydroxyl radicals (•OH) is proposed in Scheme 1 (see Fig. 5).

### *3.2 Photocatalytic activities of Pd/TNTs nanocomposites*

The photocatalytic activity of Pd/TNTs nanocomposites is evaluated by measuring the concentration of MB under simulated sunlight and is shown in Fig. 6. As shown in Fig. 6a, the photocatalytic degradation of MB is carried out without any catalyst in the blank experiment, and no obvious change in the MB solution is observed. $TiO_2$ NPs with an average diameter of 25 nm (P25) show a certain photocatalytic capacity under simulated sunlight using an iodine-tungsten lamp, because the wavelength range is from 350 to 1000 nm, which covers the absorption range of $TiO_2$ NPs (<387 nm). The photocatalytic capacity of TNTs is improved and is better than P25 due to the larger surface area of TNTs, leading to a better adsorption capacity. Compared with TNTs, Pd/TNTs nanocomposites show outstanding photocatalytic capacity. Through only 10 min irradiation, the degradation ratio of MB reaches 96.0%. The degradation ratio of MB by Pd/TNTs nanocomposites assisted by *S. oneidensis* MR-1 can be further enhanced to 98.7% in only 10 min. Fig. 6b shows the absorbance curves of MB in the photocatalysis process by Pd/TNTs nanocomposites (1 wt% of Pd) assisted by *S. oneidensis* MR-1. The absorbance value of MB at the maximum wavelength (664 nm) decreases abruptly after 10 min in the photocatalysis process and there is only very small absorbance value of MB after 50 min photocatalysis. The same results can also be obtained through comparison of the colour change of the solution. The photocatalytic capacities of Pd/TNTs nanocomposites with three different mass percentages of Pd (1, 4 and 8 wt%) are investigated;

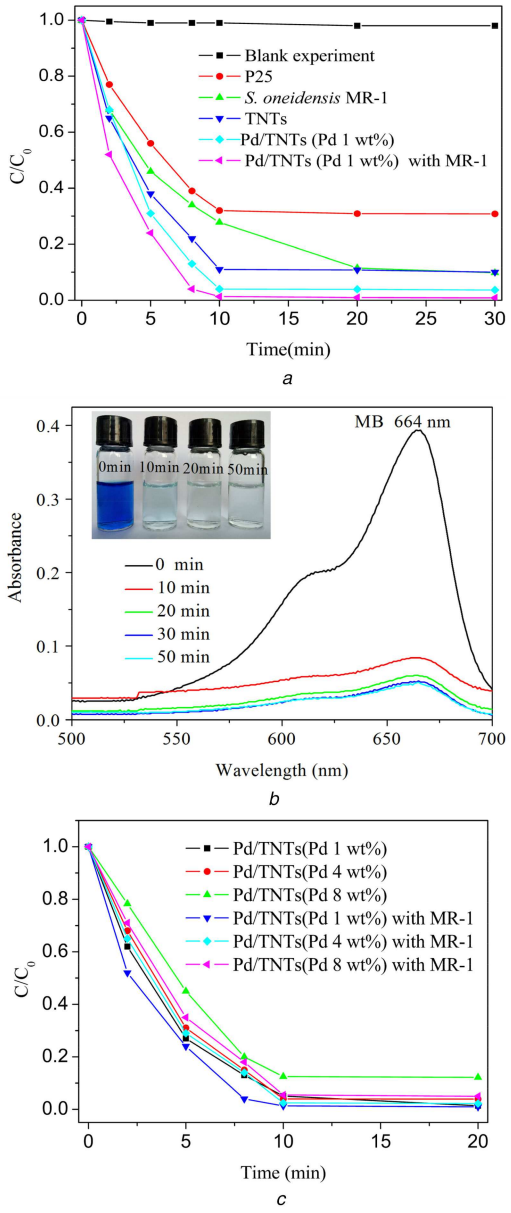


**Fig. 6** *Visible-light photocatalytic degradation curves of MB by different catalysts*

***(a)*** Photocatalytic degradation of MB by P25, TNTs, Pd/TNTs nanocomposites (1 wt% of Pd) and Pd/TNTs nanocomposites (1 wt% of Pd) assisted by *S. oneidensis* MR-1 ($5 \times 10^6$ CFU $mL^{-1}$), ***(b)*** absorbance curves of MB in the photocatalysis process by Pd/TNTs nanocomposites (1 wt% of Pd) assisted by *S. oneidensis* MR-1 ($5 \times 10^6$ CFU $mL^{-1}$), ***(c)*** Photocatalytic degradation of MB by Pd/TNTs nanocomposites (1, 4 and 8 wt% of Pd) and Pd/TNTs nanocomposites (1, 4 and 8 wt% of Pd) assisted by *S. oneidensis* MR-1 ($5 \times 10^6$ CFU $mL^{-1}$)

and the results (in Fig. 6c) show the best photocatalytic capacity of Pd/TNTs nanocomposites with lower percentages of Pd (1 wt%). A possible reason is that the higher surface coverage of Pd NPs decreases the accessibility of the active sites inside the TNTs reported by Mohapatra [29]. The results in Fig. 6c show a comparison of the photocatalytic capacities of three Pd/TNTs nanocomposites with different mass percentages of Pd (1, 4 and 8 wt%) all enhanced by assistance with *S. oneidensis* MR-1.

Due to the local electric-field enhancement, higher utilisation of sunlight and the Schottky barrier at the interface, more light-excited electrons and holes generate, separate and transfer to the surfaces of Pd/TNTs nanocomposites compared with single $TiO_2$ nanomaterials, and more hydroxyl radicals (•OH) are generated to enhance the degradation of MB adsorbed on the surface of Pd/TNTs nanocomposites. The huge surface area of the nanotubes induces the adsorption of a greater number of MB molecules,

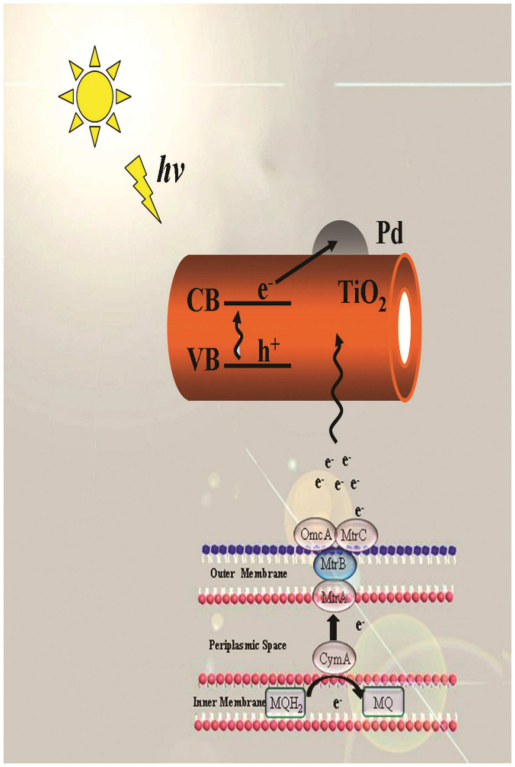


**Fig. 7** *Schematic illustration of the mechanism of photocatalytic activity for MB by Pd/TNTs nanocomposites and the synergistic effect of S. oneidensis MR-1*

which also enhances the photocatalytic efficiency of Pd/TNTs nanocomposites. For these reasons, the photocatalytic efficiency of Pd/TNTs nanocomposites is better than that of TNTs, and $TiO_2$ NPs exhibited the worst efficiency.

In our studies, *S. oneidensis* MR-1 plays two important roles, both in synthesis of Pd NPs and in the photocatalytic degradation of MB. Electrons generated in *S. oneidensis* MR-1 transfer through breathing passages to Pd/TNTs nanocomposites and take part in the degradation of MB. With the help of *S. oneidensis* MR-1, Pd/TNTs nanocomposites exhibit superior photocatalytic capacity. The same results have been reported in previous studies. The whole photocatalysis mechanism of Pd/TNTs nanocomposites and the synergistic effect of *S. oneidensis* MR-1 are shown in Fig. 7.

## 4 Conclusion

Spherical Pd NPs measuring ~6–8 nm in diameter are prepared in situ on the TNTs surface with the help of *S. oneidensis* MR-1 under benign conditions to form a heterojunction structure with TNTs. The Pd/TNTs nanocomposites show much higher photocatalytic efficiency than single TNTs and P25 under simulated sunlight in the degradation of MB. This improved efficiency, which is due to local electric-field enhancement, higher utilisation of sunlight and a Schottky barrier at the interface of Pd/TNTs nanocomposites. In the reduction of $Pd^{2+}$, *S. oneidensis* MR-1 acts as an electron donor. Conversely, *S. oneidensis* MR-1 assists Pd/TNTs nanocomposites in the photocatalytic degradation of MB, and the degradation ratio of MB reaches 98.7% after only 10 min. Such a promising bacterially based synthesis procedure may provide valuable implications for combining green synthesis of nanocomposites with contaminant biodegradation.

## 5 Acknowledgment

The authors wish to thank the National Natural Science Foundation of China (grant no. 51278001) for supporting this work.

## 6 References


[1] Heidelberg, J.F., Paulsen, I.T., Nelson, K.E., *et al.*: 'Genome sequence of the dissimilatory metal ion-reducing bacterium *Shewanella oneidensis*', *Nat. Biotechnol.*, 2002, **20**, pp. 1118–1123

[2] Suresh, A.K., Pelletier, D.A., Wang, W., *et al.*: 'Silver nanocrystallites: biofabrication using *Shewanella oneidensis*, and an evaluation of their comparative toxicity on gram-negative and gram-positive bacteria', *Environ. Sci. Technol.*, 2010, **44**, pp. 5210–5215

[3] Suresh, A.K., Pelletier, D.A., Wang, W., *et al.*: 'Biofabrication of discrete spherical gold nanoparticles using the metalreducing bacterium *Shewanella oneidensis*', *Acta Biomater.*, 2011, **7**, pp. 2148–2152

[4] Wang, H., Law, N., Pearson, G., *et al.*: 'Impact of silver(I) on the metabolism of *Shewanella oneidensis*', *J. Bacteriol.*, 2010, **192**, pp. 1143–1150

[5] Xiao, X., Zhu, W.W., Yuan, H., *et al.*: 'Biosynthesis of FeS nanoparticles from contaminant degradation in one single system', *Biochem. Eng. J.*, 2016, **105**, pp. 214–219

[6] Smith, Y.R., Ray, R.S., Carlson, K., *et al.*: 'Self-ordered titanium dioxide nanotube arrays: anodic synthesis and their photo/electro-catalytic applications', *Materials*, 2013, **6**, pp. 2892–2957

[7] Subramanian, V.R., Sarker, S., Yu, B.W., *et al.*: 'Tio$_2$ nanotubes and its composites: photocatalytic and other photo-driven applications', *J. Mater. Res.*, 2013, **28**, pp. 280–293

[8] Huang, K.C., Chien, S.H.: 'Improved visible-light-driven photocatalytic activity of rutile/titania-nanotube composites prepared by microwave-assisted hydrothermal process', *Appl. Catal. B: Environ.*, 2013, **140**, pp. 283–288

[9] Zhang, M., Wu, J., Hou, J., *et al.*: 'Molybdenum and nitrogen Co-doped titanium dioxide nanotube arrays with enhanced visible light photocatalytic activity', *Sci. Adv. Mater.*, 2013, **5**, pp. 535–541

[10] Jing, L., Zhou, W., Tian, G., *et al.*: 'Surface tuning for oxide-based nanomaterials as efficient photocatalysts', *Chem. Soc. Rev.*, 2013, **42**, pp. 9509–9549

[11] Zhang, Q., Lima, D.Q., Lee, I., *et al.*: 'A highly active titanium dioxide based visible-light photocatalyst with nonmetal doping and plasmonic metal decoration', *Angew Chem. Int. Ed.*, 2011, **50**, pp. 7088–7092

[12] Gomathi Devi, L., Kavitha, R.: 'A review on plasmonic metal $TiO_2$ composite for generation, trapping, storing and dynamic vectorial transfer of photogenerated electrons across the Schottky junction in a photocatalytic system', *Appl. Surf. Sci.*, 2016, **360**, pp. 601–622

[13] Yang, D., Sun, Y.Y., Tong, Z.W., *et al.*: 'Synthesis of Ag/$TiO_2$ nanotube heterojunction with improved visible-light photocatalytic performance inspired by bioadhesion', *J. Phys. Chem. C*, 2015, **119**, pp. 5827–5835

[14] Chen, Q.H., Xin, Y.J., Zhu, X.W.: 'Au-Pd nanoparticles-decorated $TiO_2$ nanobelts for photocatalytic degradation of antibiotic levofloxacin in aqueous solution', *Electrochim. Acta*, 2015, **186**, pp. 34–42

[15] Magdalena, D., Ewelina, G., Adriana, Z.: 'Synthesis, characterization and photocatalytic activity of noble metal-modified $TiO_2$ nanosheets with exposed {0 0 1} facets', *Appl. Surf. Sci.*, 2015, **347**, pp. 275–285

[16] Hou, W.B., Cronin, S.B.: 'A review of surface plasmon resonance-enhanced photocatalysis', *Adv. Funct. Mater.*, 2012, **23**, pp. 1612–1619

[17] Zhang, Z.H., Yu, Y.J., Wang, P.: 'Hierarchical top-porous/bottom-tubular $TiO_2$ nanostructures decorated with Pd nanoparticles for efficient photoelectrocatalytic decomposition of synergistic pollutants', *ACS Appl. Mater. Interfaces*, 2012, **4**, pp. 990–996

[18] Assaud, L., Brazeau, N., Barr, M.K.S., *et al.*: 'Atomic layer deposition of Pd nanoparticles on $TiO_2$ nanotubes for ethanol electrooxidation: synthesis and electrochemical properties', *ACS Appl. Mater. Interfaces*, 2015, **7**, pp. 24533–24542

[19] Honciuc, A., Laurin, M., Albu, S., *et al.*: 'Controlling the adsorption kinetics via nanostructuring: Pd nanoparticles on $TiO_2$ nanotubes', *Langmuir*, 2010, **26**, pp. 14014–14023

[20] Wang, W.Z., Varghese, O.K., Paulose, M., *et al.*: 'A study on the growth and structure of titania nanotubes', *J. Mater. Res.*, 2004, **19**, pp. 417–422

[21] Lim, S.H., Luo, J.Z., Zhong, Z.Y., *et al.*: 'Room-temperature hydrogen uptake by $TiO_2$ nanotubes', *Inorg. Chem.*, 2005, **44**, pp. 4124–4126

[22] Mohapatra, S.K., Misra, M., Mahajan, V.K., *et al.*: 'Design of a highly efficient photoelectrolytic cell for hydrogen generation by water splitting: application of $TiO_{2-x}C_x$ nanotubes as a photoanode and Pt/$TiO_2$ nanotubes as a cathode', *J. Phys. Chem. C*, 2007, **111**, pp. 8677–8685

[23] Xiong, Y., Chen, J., Wiley, B., *et al.*: 'Size-dependence of surface plasmon resonance and oxidation for Pd nanocubes synthesized via a seed etching process', *Nano. Lett.*, 2005, **5**, pp. 1237–1242

[24] Xiong, Y., McLellan, J.M., Chen, J., *et al.*: 'Kinetically controlled synthesis of triangular and hexagonal nanoplates of palladium and their SPR/SERS properties', *J. Am. Chem. Soc.*, 2005, **127**, pp. 17118–17127

[25] Wang, J.G., Rao, P.H., An, W., *et al.*: 'Boosting photocatalytic activity of Pd decorated $TiO_2$ nanocrystal with exposed (001) facets for selective alcohol oxidations', *Appl. Catal. B: Environ.*, 2016, **195**, pp. 141–148

[26] Huang, H., Leung, D.Y.C.: 'Complete oxidation of formaldehyde at room temperature using $TiO_2$-supported metallic Pd nanoparticles', *ACS Catal.*, 2011, **1**, pp. 348–354

[27] Ouyang, L., Da, G.J., Tian, P.F., *et al.*: 'Insight into active sites of Pd-Au/$TiO_2$ catalysts in hydrogen peroxide synthesis directly from $H_2$ and $O_2$', *J. Catal.*, 2014, **311**, pp. 129–136

[28] Le, F., Brandl, D.W., Urzhumov, Y.A., *et al.*: 'Metallic nanoparticle arrays: A common substrate for both surface-enhanced Raman scattering and surface-enhanced infrared absorption', *ACS Nano*, 2008, **2**, pp. 707–718

[29] Mohapatra, S.K., Kondamudi, N., Banerjee, S., *et al.*: 'Functionalization of self-organized $TiO_2$ nanotubes with Pd nanoparticles for photocatalytic decomposition of dyes under solar light illumination', *Langmuir*, 2008, **24**, pp. 11276–11281